Structural Measures as Guides to Ultrastable States in Overjammed Packings

Sangwoo Kim
Department of Mechanical Engineering, University of California Santa Barbara, Santa Barbara, California 93106-5070, USA

Sascha Hilgenfeldt
Department of Mechanical Science and Engineering, University of Illinois at Urbana-Champaign, Urbana, Illinois 61801, USA

(Received 1 March 2022; revised 18 May 2022; accepted 19 September 2022; published 11 October 2022)

Jammed, disordered packings of given sets of particles possess a multitude of equilibrium states with different mechanical properties. Identifying and constructing desired states, e.g., of superior stability, is a complex task. Here, we show that in two-dimensional particle packings the energy of all metastable states (inherent structures) is reliably classified by simple scalar measures of local steric packing. These structural measures are insensitive to the particle interaction potential and so robust that they can be used to guide a modified swap algorithm that anneals polydisperse packings toward low-energy metastable states exceptionally fast. The low-energy states are extraordinarily stable against applied shear, so that the approach also efficiently identifies ultrastable packings.

DOI: 10.1103/PhysRevLett.129.168001

Modern materials science has developed and explored materials with an unprecedented variety of properties and applications. Much of this vast expansion of the field concerns matter with nontrivial structure, such as metamaterials, glasses, or amorphous solids. The building blocks of these materials can range from atoms to the macroscopic, but regardless of scale the mechanical behavior of interest stems from the disordered arrangement of constituents.

Many modeling approaches to disordered matter construct a mechanical energy functional based on primary physical forces between the constituents, resulting in highly complex, multidimensional energy landscapes, where even the ground state is hard to determine or to merely prove to exist [1]. Beyond the ground state, a huge number of local minima are found (metastable states, MS), equivalently called inherent structures in glasses and supercooled liquids [2,3] [Fig. 1(a)]. The mechanical properties of MS can vary significantly, often in correlation with the energy of the state. Given the intricacies of the energy landscape, being able to identify and construct MS with desired mechanical properties (such as extraordinary stability) is a formidable task of great current interest [4,5]. In the present Letter, we will show that, in a large class of soft-disk packings, (i) easily evaluated structural measures are strong indicators of MS energy, (ii) low MS energy correlates strongly with mechanical ultrastability, and (iii) using the structural measures as a guide, an efficient algorithm is developed that constructs such states of very low energy and very high stability much faster than previous approaches.

Our current work on packings is inspired by previous findings in two-dimensional (2D) domain systems (consisting of space-filling polygonal domains, such as dry foams or confluent biological tissues). There, the mechanical energy functional can be quantified by features of the domain structure such as the distribution of the shortest edges between the 2D domains [6] or the statistical moments of the distributions of domain size and topology [7]. For soft disk packings, we explore different measures and their ability to predict mechanical energy: (1) mean number of contacts z, the average over the number of contacts z_i for each particle [Fig. 1(b)]; (2) gap fraction ϕ_g, from the sum of the disjoint areas not covered by

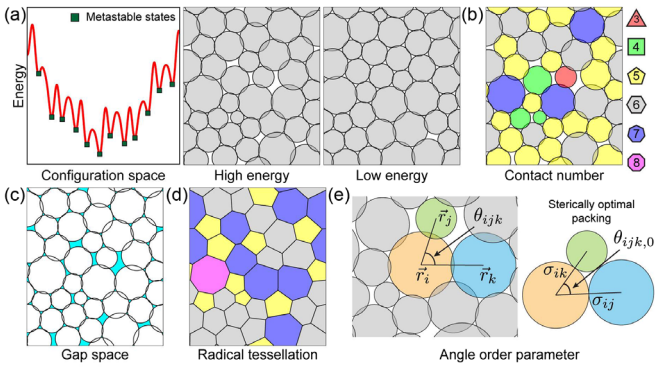

FIG. 1. (a) Schematic energy landscape of disordered systems and two example packing metastable states of high energy (left) and low energy (right). Structural measures of metastable particle configurations: (b) contact number (color coded); (c) gap space; (d) radical tessellation to compute equivalent foam energy; and (e) local steric angles for computation of the angle order parameter.

potentially overlapping disks [Fig. 1(c)]; (3) equivalent foam energy ϵ_f^*, the normalized sum of the perimeters of radical tessellation cells constructed around particle centers and weighted by particle area [Fig. 1(d)], cf. [6,7]; (4) an angle order parameter Θ adapted from the literature on glasses [8,9] [Fig. 1(e)] and defined in Eq. (1) below. This last measure most explicitly captures the structural closeness of a given MS to a sterically optimal packing that distinguishes high-energy MS from low-energy MS.

For every triplet of disks i, j, k in a packing that are mutual neighbors by radical tessellation, θ_{ijk} is the angle between centroid connectors, while $\theta_{ijk,0}$ is the same angle assuming perfect local steric packing [all three particles touch, see Fig. 1(e)]. Averaging angular deviations over the n_i triplets involving particle i, then over all particles, defines

$$\Theta = \frac{1}{N}\sum_{i=1}^{N}\frac{1}{n_i}\sum_{j,k}|\theta_{ijk} - \theta_{ijk,0}|, \tag{1}$$

see Supplemental Material [10] for further details.

A host of studies has focused on particle systems at the point of jamming [11–15], where analogies to critical phenomena are apparent [16–18]. When hard particles assemble or aggregate, they are usually trapped in states very close to that of critical jamming at a volume fraction ϕ_J [12,19], whose exact value depends on protocol [20,21]. On the other hand, a system of soft particles can be compressed significantly beyond ϕ_J. We investigate the energy landscape in this overjammed case, using a repulsive harmonic particle model, cf. [22–25]. Constituent particles are frictionless soft disks that interact if there is physical contact between them. The dimensionless energy functional of a system of N disks is

$$\epsilon_r = \frac{1}{3N}\sum_{i,j}\frac{1}{2}\left(1 - \frac{r_{ij}}{\sigma_{ij}}\right)^2 H\left(1 - \frac{r_{ij}}{\sigma_{ij}}\right) - \epsilon_{r,0}, \tag{2}$$

$$\epsilon_{r,0} = \frac{1}{2}[1 - (2\sqrt{3}\phi/\pi)^{-1/2}]^2, \tag{3}$$

where r_{ij} is the distance between particle i and j and $H(\cdot)$ is the Heaviside step function. The equilibrium distance σ_{ij} is chosen consistent with the particle areas A_i and equivalent circle radii $\sigma_i = \sqrt{A_i/\pi}$, i.e., $\sigma_{ij} = \sigma_i + \sigma_j$. The area fraction ϕ is set to 1 throughout, both for definiteness and for a closer analog to domain systems, where $\phi = 1$ by definition. Limited results with $0.95 \le \phi \le 1.1$ have been obtained and do not change the conclusions presented here. For a given ϕ, $\epsilon_{r,0}$ is the reference energy of a regular hexagonal packing of monodisperse particles. We emphasize that none of the following results are sensitive to the particular potential (2), see Supplemental Material [10] for example results using a repulsive Hertzian potential instead.

To access a wide spectrum of disorder, initial disk positions are generated from various point generation schemes: perturbed lattice algorithm [26,27], hard-core algorithm [28], and Lloyd algorithm [29]. Tuning control parameters in each scheme constructs a multitude of initial states with distinct positional disorder in a periodic simulation domain. Each initial configuration is annealed by the FIRE algorithm [30], finding the nearest MS (minimum of ϵ_r). In the following, we will first focus on monodisperse packings, then on the polydisperse case.

Monodisperse structures have a known ground state, the regular hexagonal packing. Simulations with different initial positional disorder from regular hexagonal lattice points to random Poisson points produce a complete range of MS energies ϵ_r from 0 (ground state) to a well-defined maximum, where higher-energy states become exponentially rare [Figs. 2(b)–2(e)]; this range reduces only mildly with increased system size (see Supplemental Material [10]). The discontinuity between 0 and the first $\epsilon_r > 0$ is a finite-size effect, as the latter state is characterized by the generation of the first dislocation defect pair. Each additional particle defect affects the four measures of MS structure: a defect is by definition missing contacts, leads to larger gap spaces, distorts the tessellation cell of the affected particles, and makes larger contributions to Θ.

While the most disordered initial conditions tend to relax to the highest MS energies, even in those MS the majority of particles are locally hexagonally coordinated, so that the equilibrium density of topological defects is small, and their types restricted to isolated dislocations, vacancy defects, or scar defects [31], see Fig. 2(a). This is in stark contrast to monodisperse domain systems, where the highest-energy MS are thoroughly disordered, amorphous

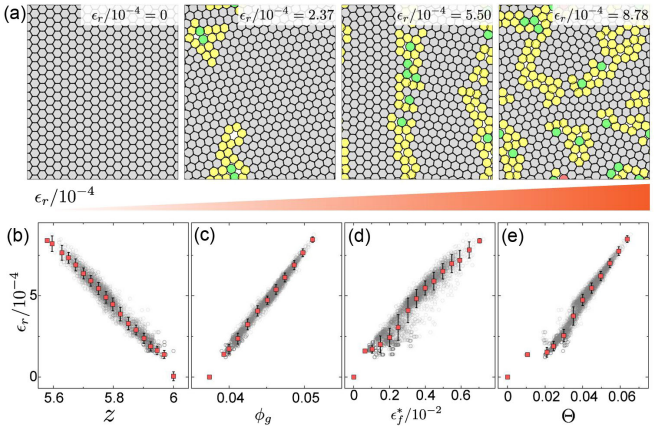

FIG. 2. (a) Example metastable states for the monodisperse particle system, $N = 400$, metastable energy increases from left to right. Each particle is color coded by contact number. Structural measures correlating with MS energy: (b) contact number, (c) gap space, (d) equivalent foam energy, and (e) angle order parameter. Gray symbols are individual MS ($n = 5000$ samples), red symbols are binned mean and standard deviation.

structures without any local hexagonal arrangement. Accordingly, the range of equivalent foam energies ϵ_f^* in the particle system [Fig. 2(d)] is about a factor of 6 smaller than in the domain case [7]—the two cases are directly comparable as the monodisperse particle ground state directly translates via tessellation to the honeycomb ground state of the domain system.

All four structural measures show a strong linear correlation with MS energy, so that they can be used as alternative indicators of energy. Interestingly, the correlation of ϵ_r with ϵ_f^* is poorer than with the other measures, indicating that a translation to domains is not the most advantageous approach to quantifying MS energies.

To avoid spontaneous crystallization, particle polydispersity is often introduced. In the following, we study the MS energy spectrum of particle packings with a continuous area polydispersity of $c_A \equiv \langle (A-1)^2 \rangle^{1/2} = 0.4$ (radius polydispersity $c_R \approx 0.2$), randomly assigning N particle area values from a gamma distribution with mean $\langle A \rangle = 1$ and coefficient of variation c_A. Unlike in the monodisperse system, the ground state is unknown, and all metastable states represent amorphous structures with a finite fraction of topological defects, cf. Fig. 3(a). Using a different unimodal distribution (e.g., Gaussian, log normal) with the same mean and c_A yields near-identical results (see Supplemental Material [10]).

We find that, contrary to monodisperse packings, varying initial positional disorder as widely as possible is not sufficient to explore the entire range of possible MS energies, but only produces a narrow interval of high-energy MS on the landscape of polydisperse systems [gray in Figs. 3(b)–3(e)]. To find lower-energy MS, we simplify a particle swap algorithm from glassy systems [32,33], exclusively using random Monte Carlo (MC) particle area swaps with ensuing FIRE relaxation, accepting the swap if the energy decreases. This algorithm [Fig. 4(a)] produces MS energy values ranging dramatically lower [magenta in Figs. 3(b)–3(e)] than the positional-disorder computations. While there might be spatially correlated states of even lower energy [34], the vast majority of the polydisperse MS energy range is probed here. Note that the smallest polydisperse ϵ_r are slightly negative, as their energy is below that of the monodisperse ground state.

All four scalar measures again strongly correlate with MS energy [Figs. 3(b)–3(e)], so that these measures can be used to diagnose relative energy levels of MS from a

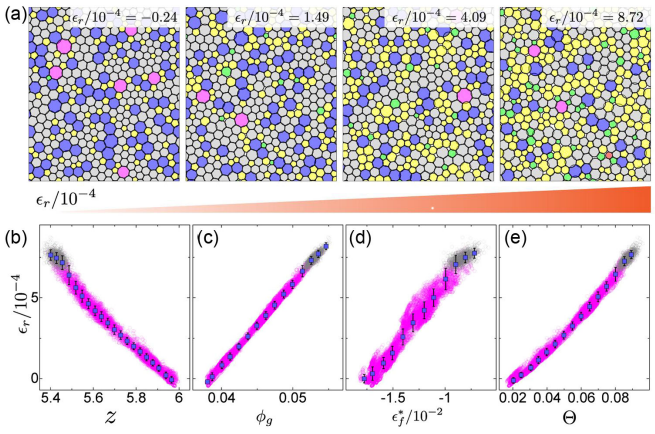

FIG. 3. (a) Example metastable states for the polydisperse particle system, $c_A = 0.4$ and $N = 400$, metastable energy increases from left to right. Each particle is color coded by contact number. Structural measures correlating with MS energy: (b) contact number, (c) gap space, (d) equivalent foam energy, and (e) angle order parameter. Gray points result from annealing different initial configurations to the nearest MS ($n = 9000$ samples), and magenta points are obtained by the Monte Carlo swap algorithm ($n = 173\,000$). Blue symbols are binned mean and standard deviation.

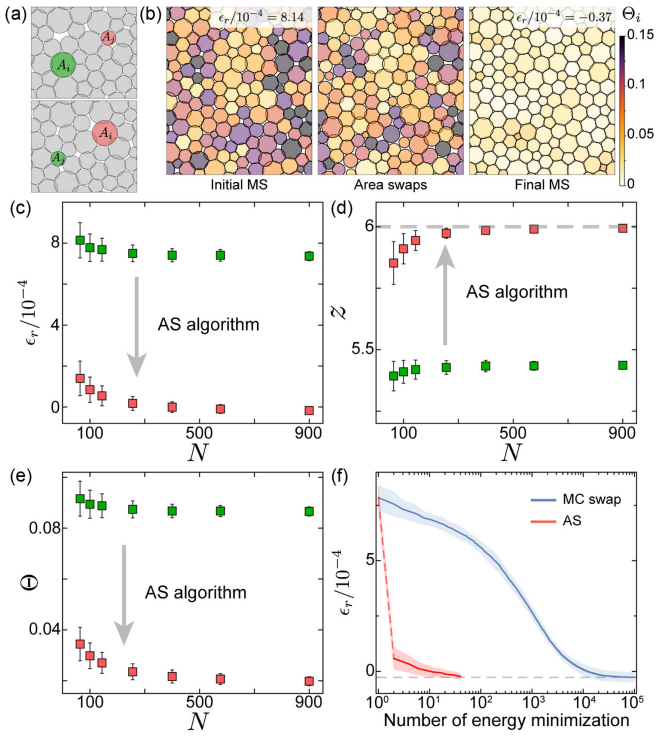

FIG. 4. (a) Schematic showing a single area swap between particles i and j. (b) A simultaneous area swap algorithm to minimize the angle order parameter, demonstrated for $N = 144$. Individual particles are color coded in terms of their Θ_i values. (c) Energy ϵ_r, (d) mean number of contacts z, and (e) angle order parameter Θ of MS obtained by the angle swap algorithm for different system sizes, average over 1000 MS for each N. Green and red data points represent initial and final MS, respectively. (f) Angle swap simulations reduce energy far faster than Monte Carlo swap simulations. Mean and standard deviation of energies of 50 initially random packings are shown against number of FIRE energy minimizations. Blue: MC swap; the gray dashed line indicates the MC mean energy after 10^5 steps. Red: AS algorithm, reaching this energy after 40 steps.

snapshot of overjammed polydisperse particle packings. That all correlations are nearly linear may indicate that the packing constraint of volume fraction is so strong that all possible MS can be interpreted as small perturbations of the lowest-energy state, represented by a Taylor expansion in each structural parameter. Again, the measures most directly related to the quality of steric packing show better correlation, and thus more predictive power, than the domain-related measure ϵ_f^*. Furthermore, accurate empirical measurements of tessellation topology in an experimental system are easier to obtain than those of contact topology or gap fraction, which depend sensitively on small-scale details of touching or near-touching particles. Hence, the angle order parameter Θ should predict MS energy from experimental snapshots most robustly. In contrast to the global measure Θ, the local deviations of individual particles from perfect steric packing do not correlate well with their contributions to ϵ_r (see Supplemental Material [10]).

In seminal work on particle systems near the jamming point, a universal scaling relating the volume fraction and z is reported [22,24]. In the present study (where $\phi = 1$ for all samples), a relatively well-defined z is valid for states obtained by variation of initial conditions [high-energy states, gray in Fig. 3(b)]. But when taking states from the entire range of MS energies into account, we see that MS indeed exist for a wide range of z values at *fixed* area fraction.

The lowest-energy states of such overjammed systems (approaching the upper limit $z \to 6$, cf. Fig. 3(b) are of particular interest, as they constitute rare and unusual configurations with exceptional mechanical properties.

We will show below that they indeed represent ultrastable states of the material [4,5,35–40]. Finding these rare states is challenging and resource intensive, even via MC swap simulations. However, our structural measures, beyond their diagnostic usefulness, suggest a much more efficient way of finding low-energy MS using the quality of steric packing as a guide.

We here present a highly efficient swap algorithm to lower MS energy, guided by minimization of the angle order parameter Θ. For an initial MS with given particle sizes $\{A_i\}$ and radical tessellation topologies $\{n_i\}$, there exists a unique set of particle areas $\{C_i\}$ for which the packing is sterically optimal everywhere, while preserving the topologies $\{n_i\}$. This structure is computed by the circle packing algorithm [41] and, by construction, has $\Theta = 0$. The distribution $\{C_i\}$ does not match $\{A_i\}$, but ordering both sets by size, we can reassign the $\{A_i\}$ to the positions of the $\{C_i\}$ matching relative size. The result is a very fast, simultaneous swap of all $\{A_i\}$ areas [cf. Fig. 4(b)]. The system is annealed to the nearest MS after the area reassignment and this reassignment step is repeated until the tessellation topology remains fixed. We will refer to this as the angle swap (AS) algorithm. As the AS algorithm inherently fixes the particle packing topology, we then randomize the positions of all particles again, find the nearest MS (one FIRE step), and perform another AS. If this second application of AS lowers the energy below that of the first, it is accepted, otherwise rejected, analogous to the MC swap algorithm. Applying pairs of randomization and AS steps multiple times reaches lower MS energies by exploring distinct packing topologies.

The vast majority of metastable states require only a single simultaneous area swap for the AS algorithm to terminate. The resulting state invariably proves to have very low Θ and very low energy [Figs. 4(c)–4(e)]. Thus, only one FIRE energy minimization is needed to obtain a low-energy MS—this is reminiscent of recent work that achieves approximate simultaneous rearrangement in a single step by introducing transient degrees of freedom [5]. Attempts to implement a similar swap algorithm guided by the z or ϕ_g measures do not lead to such fast termination. As the system size increases, the MS obtained by angle swap tends to show lower energy, larger z, and smaller Θ, as a larger set of area values reduces the discrepancy between the reassigned particle sizes $\{A_i\}$ and the sterically optimal circle packing sizes $\{C_i\}$ [Figs. 4(c)–4(e)].

In Fig. 4(f), we compare the performance of the MC and AS algorithms in achieving the lowest energies. MC annealing is performed for 50 samples with random initial conditions; the energy decrease saturates after about 10^5 MC swaps, each needing one FIRE minimization. For AS, 50 random initial conditions are first annealed by the AS algorithm, immediately reaching much lower energies [dashed line in Fig. 4(f)]. Then the alternating randomization and AS steps are successively applied to lower MS energy further. We find that the AS algorithm requires only 20 such randomization-AS steps (40 FIRE minimizations in total) to reach energies as low as those obtained with 10^5 MC swaps, i.e., the computational effort is about 2500 times smaller. Furthermore, the computational advantage of the AS algorithm over MC swap becomes even greater for increasing system size (see Supplemental Material [10]). All of this suggests that the AS protocol proposed here is extraordinarily efficient in identifying low-energy MS, the ideal candidates for rare ultrastable states.

To show that low-energy states are exceptionally stable, mechanical stability needs to be assessed. One method inspired by scaling laws of states near the jamming point [18,42] is to quantify virial system pressure P [43,44] as a measure for isotropic stress needed to destabilize the packing. We find that for both monodisperse and polydisperse MS, P correlates strongly with ϵ_r, so that low-energy states are most stable (see Supplemental Material [10]).

A more direct and practical probe of MS stability is to assess sensitivity to shear deformation. Thus, we apply pure shear strain incrementally and quasistatically [minimizing

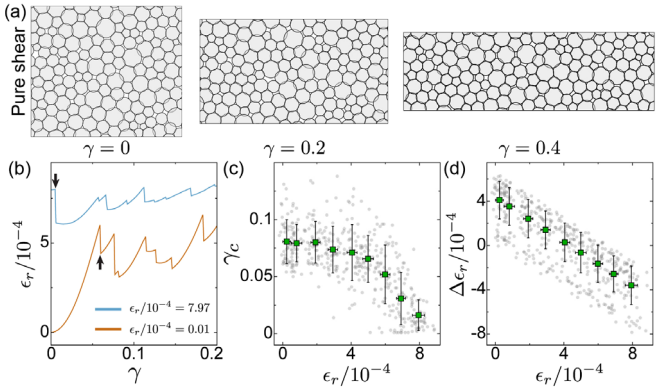

FIG. 5. (a) Schematics of pure shear simulations. (b) Examples of energy as a function of strain starting at high (cyan) and low (brown) energy. Strain values γ_c for the first irreversible rearrangement are indicated by arrows. (c) Critical strain γ_c as a function of state energy ϵ_r. (d) Energy difference between final MS and initial MS induced by irreversible rearrangement. Gray symbols are individual MS ($n = 450$), colored symbols are binned mean and standard deviation.

energy after every strain step, Fig. 5(a)], and track MS energy variations as well as structural rearrangements (note that for our overjammed states we do not vary shear direction or box shape, which may be influential factors closer to the jamming transition [45]).

All metastable states initially exhibit an increase of energy due to applied strain and then intermittent finite energy drops due to irreversible particle rearrangements [Fig. 5(b)]. The first such relaxation event defines a critical strain γ_c that measures stability [46]. While the effect of the first contact change on the shear modulus near the jamming point has been studied [47,48], the critical strain defined here involves plastic rearrangement of particles, so that the MS after one cyclic shear deformation is irreversibly changed. Figure 5(b) shows a typical example of shearing a high-energy initial state vs shearing the low-energy state resulting from it through the AS algorithm, demonstrating that γ_c of the latter has increased drastically. Regardless of how an MS is constructed, a strong correlation between its energy and γ_c is found [Fig. 5(c)]. This implies that the typical energy well of low-energy MS minima is significantly deeper.

As may be expected intuitively, for the highest-energy states $\gamma_c \to 0$, while for lower MS energy critical strain saturates to a plateau value γ_{cp}, stretching over nearly half of the range of MS energies [Fig. 5(c)]. Low-energy MS for lower volume fractions exhibit nearly the same γ_{cp} (see Supplemental Material [10]), indicating that the superior mechanical stability of these low-energy states persists close to the jamming transition.

Considering the difference $\Delta\epsilon_r$ between the MS energies after and before the rearrangement induced by the γ_c shear strain [Fig. 5(d)], we see that the rearrangement lowers the energy only for the higher-energy initial states. By contrast, the most stable, low-energy MS with $\gamma_c \approx \gamma_{cp}$ transition to higher energy ($\Delta\epsilon_r > 0$). This indicates that periodic shear strain, while a common strategy to anneal configurations of particles or domains [49–51], will not efficiently reduce energy toward the lowest values. To obtain the latter, more sophisticated particle rearrangement strategies like AS are necessary.

Through the robust correlations of structural measures with MS energies, and further with mechanical stability, a simple snapshot of an experimental system can thus be used to diagnose its stability without mechanical tests. Our description of the MS energy landscape extends the geometric principle of the granocentric model [52–54], which describes ground states as those of optimal steric packing. Measures like Θ quantify MS with all realizable energies, and provide algorithms for their construction.

Beyond diagnostics, the angle swap algorithm developed here is able to construct ultrastable states more efficiently than previous efforts. Finding such states is an objective of recent experiments and simulations in the glass literature [4,5,35–39], for which AS could be greatly beneficial. More broadly, distinct microstructures obtained and diagnosed *in silico* by the approach detailed here can be used as blueprints to guide the design of packings with desired mechanical properties. Our algorithms can also be applied to glasses and supercooled liquids in low-temperature equilibrium states, as the latter correlate with low inherent structure energy [3,35].

The authors are grateful for helpful discussions with Rafael Blumenfeld, Jasna Brujić, and Varda Faghir Hagh, and to Kenneth Stephenson for his help with the circle packing algorithm.

[1] G. Zhang, F. H. Stillinger, and S. Torquato, Classical many-particle systems with unique disordered ground states, Phys. Rev. E **96**, 042146 (2017).
[2] Frank H. Stillinger, A topographic view of supercooled liquids and glass formation, Science **267**, 1935 (1995).
[3] Pablo G. Debenedetti and Frank H. Stillinger, Supercooled liquids and the glass transition, Nature (London) **410**, 259 (2001).
[4] Geert Kapteijns, Wencheng Ji, Carolina Brito, Matthieu Wyart, and Edan Lerner, Fast generation of ultrastable computer glasses by minimization of an augmented potential energy, Phys. Rev. E **99**, 012106 (2019).
[5] Varda F. Hagh, Sidney R. Nagel, Andrea J. Liu, M. Lisa Manning, and Eric I. Corwin, Transient learning degrees of freedom for introducing function in materials, Proc. Natl. Acad. Sci. U.S.A. **119**, e2117622119 (2022).
[6] Sangwoo Kim, Yiliang Wang, and Sascha Hilgenfeldt, Universal Features of Metastable State Energies in Cellular Matter, Phys. Rev. Lett. **120**, 248001 (2018).
[7] Sangwoo Kim and Sascha Hilgenfeldt, A simple landscape of metastable state energies for two-dimensional cellular matter, Soft Matter **15**, 237 (2019).

[8] Hua Tong and Hajime Tanaka, Revealing Hidden Structural Order Controlling Both Fast and Slow Glassy Dynamics in Supercooled Liquids, Phys. Rev. X **8**, 011041 (2018).
[9] Hajime Tanaka, Hua Tong, Rui Shi, and John Russo, Revealing key structural features hidden in liquids and glasses, Nat. Rev. Phys. **1**, 333 (2019).
[10] See Supplemental Material at http://link.aps.org/supplemental/10.1103/PhysRevLett.129.168001 for further details on simulation protocols, structural measures, and additional supporting simulation data.
[11] Corey S. O'Hern, Stephen A. Langer, Andrea J. Liu, and Sidney R. Nagel, Random Packings of Frictionless Particles, Phys. Rev. Lett. **88**, 075507 (2002).
[12] Corey S. O'Hern, Leonardo E. Silbert, Andrea J. Liu, and Sidney R. Nagel, Jamming at zero temperature and zero applied stress: The epitome of disorder, Phys. Rev. E **68**, 011306 (2003).
[13] Wouter G. Ellenbroek, Ellák Somfai, Martin van Hecke, and Wim van Saarloos, Critical Scaling in Linear Response of Frictionless Granular Packings near Jamming, Phys. Rev. Lett. **97**, 258001 (2006).
[14] Andrea J. Liu and Sidney R. Nagel, The jamming transition and the marginally jammed solid, Annu. Rev. Condens. Matter Phys. **1**, 347 (2010).
[15] S. Torquato and F. H. Stillinger, Jammed hard-particle packings: From Kepler to Bernal and beyond, Rev. Mod. Phys. **82**, 2633 (2010).
[16] Peter Olsson and S. Teitel, Critical Scaling of Shear Viscosity at the Jamming Transition, Phys. Rev. Lett. **99**, 178001 (2007).
[17] Michio Otsuki and Hisao Hayakawa, Critical scaling near jamming transition for frictional granular particles, Phys. Rev. E **83**, 051301 (2011).
[18] James D. Sartor, Sean A. Ridout, and Eric I. Corwin, Mean-Field Predictions of Scaling Prefactors Match Low-Dimensional Jammed Packings, Phys. Rev. Lett. **126**, 048001 (2021).
[19] Steven Atkinson, Frank H. Stillinger, and Salvatore Torquato, Existence of isostatic, maximally random jammed monodisperse hard-disk packings, Proc. Natl. Acad. Sci. U.S.A. **111**, 18436 (2014).
[20] Pinaki Chaudhuri, Ludovic Berthier, and Srikanth Sastry, Jamming Transitions in Amorphous Packings of Frictionless Spheres Occur over a Continuous Range of Volume Fractions, Phys. Rev. Lett. **104**, 165701 (2010).
[21] Misaki Ozawa, Ludovic Berthier, and Daniele Coslovich, Exploring the jamming transition over a wide range of critical densities, SciPost Phys. **3**, 027 (2017).
[22] D. J. Durian, Foam Mechanics at the Bubble Scale, Phys. Rev. Lett. **75**, 4780 (1995).
[23] Atsushi Ikeda, Ludovic Berthier, and Peter Sollich, Unified Study of Glass and Jamming Rheology in Soft Particle Systems, Phys. Rev. Lett. **109**, 018301 (2012).
[24] Arman Boromand, Alexandra Signoriello, Janna Lowensohn, Carlos S. Orellana, Eric R. Weeks, Fangfu Ye, Mark D. Shattuck, and Corey S. O'Hern, The role of deformability in determining the structural and mechanical properties of bubbles and emulsions, Soft Matter **15**, 5854 (2019).
[25] Hua Tong, Shiladitya Sengupta, and Hajime Tanaka, Emergent solidity of amorphous materials as a consequence of mechanical self-organisation, Nat. Commun. **11**, 4863 (2020).
[26] Valerio Lucarini, From symmetry breaking to poisson point process in 2D Voronoi tessellations: The generic nature of hexagons, J. Stat. Phys. **130**, 1047 (2008).
[27] Sangwoo Kim, Justin J. Cassidy, Boyuan Yang, Richard W. Carthew, and Sascha Hilgenfeldt, Hexagonal patterning of the insect compound eye: Facet area variation, defects, and disorder, Biophys. J. **111**, 2735 (2016).
[28] H. X. Zhu, S. M. Thorpe, and A. H. Windle, The geometrical properties of irregular two-dimensional Voronoi tessellations, Philos. Mag. A **81**, 2765 (2001).
[29] S. Lloyd, Least squares quantization in PCM, IEEE Trans. Inf. Theory **28**, 129 (1982).
[30] Erik Bitzek, Pekka Koskinen, Franz Gähler, Michael Moseler, and Peter Gumbsch, Structural Relaxation Made Simple, Phys. Rev. Lett. **97**, 170201 (2006).
[31] Pasquale Digregorio, Demian Levis, Leticia F. Cugliandolo, Giuseppe Gonnella, and Ignacio Pagonabarraga, Unified analysis of topological defects in 2D systems of active and passive disks, Soft Matter **18**, 566 (2022).
[32] Tomás S. Grigera and Giorgio Parisi, Fast Monte Carlo algorithm for supercooled soft spheres, Phys. Rev. E **63**, 045102 (2001).
[33] Andrea Ninarello, Ludovic Berthier, and Daniele Coslovich, Models and Algorithms for the Next Generation of Glass Transition Studies, Phys. Rev. X **7**, 021039 (2017).
[34] P. I. C. Teixeira, F. Graner, and M. A. Fortes, Mixing and sorting of bidisperse two-dimensional bubbles, Eur. Phys. J. E **9**, 161 (2002).
[35] Stephen F. Swallen, Kenneth L. Kearns, Marie K. Mapes, Yong Seol Kim, Robert J. McMahon, M. D. Ediger, Tian Wu, Lian Yu, and Sushil Satija, Organic glasses with exceptional thermodynamic and kinetic stability, Science **315**, 353 (2007).
[36] Yunlong Guo, Anatoli Morozov, Dirk Schneider, Jae Woo Chung, Chuan Zhang, Maike Waldmann, Nan Yao, George Fytas, Craig B. Arnold, and Rodney D. Priestley, Ultrastable nanostructured polymer glasses, Nat. Mater. **11**, 337 (2012).
[37] Sadanand Singh, M. D. Ediger, and Juan J. de Pablo, Ultrastable glasses from *in silico* vapour deposition, Nat. Mater. **12**, 139 (2013).
[38] Misaki Ozawa, Ludovic Berthier, Giulio Biroli, Alberto Rosso, and Gilles Tarjus, Random critical point separates brittle and ductile yielding transitions in amorphous materials, Proc. Natl. Acad. Sci. U.S.A. **115**, 6656 (2018).
[39] Wei-Ting Yeh, Misaki Ozawa, Kunimasa Miyazaki, Takeshi Kawasaki, and Ludovic Berthier, Glass Stability Changes the Nature of Yielding under Oscillatory Shear, Phys. Rev. Lett. **124**, 225502 (2020).
[40] Taiki Yanagishima, John Russo, Roel P. A. Dullens, and Hajime Tanaka, Towards Glasses with Permanent Stability, Phys. Rev. Lett. **127**, 215501 (2021).
[41] K. Stephenson, *Introduction to Circle Packing: The Theory of Discrete Analytic Functions* (Cambridge University Press, Cambridge, England, 2005).

[42] Carl P. Goodrich, Andrea J. Liu, and Sidney R. Nagel, Solids between the mechanical extremes of order and disorder, Nat. Phys. **10**, 578 (2014).
[43] D. H. Tsai, The virial theorem and stress calculation in molecular dynamics, J. Chem. Phys. **70**, 1375 (1979).
[44] J. A. Zimmerman, E. B. Webb III, J. J. Hoyt, R. E. Jones, P. A. Klein, and D. J. Bammann, Calculation of stress in atomistic simulation, Model. Simul. Mater. Sci. Eng. **12**, S319 (2004).
[45] Simon Dagois-Bohy, Brian P. Tighe, Johannes Simon, Silke Henkes, and Martin van Hecke, Soft-Sphere Packings at Finite Pressure but Unstable to Shear, Phys. Rev. Lett. **109**, 095703 (2012).
[46] Francesco Arceri, Eric I. Corwin, and Varda F. Hagh, Marginal stability in memory training of jammed solids, Phys. Rev. E **104**, 044907 (2021).
[47] Merlijn S. van Deen, Johannes Simon, Zorana Zeravcic, Simon Dagois-Bohy, Brian P. Tighe, and Martin van Hecke, Contact changes near jamming, Phys. Rev. E **90**, 020202 (2014).
[48] Merlijn S. van Deen, Brian P. Tighe, and Martin van Hecke, Contact changes of sheared systems: Scaling, correlations, and mechanisms, Phys. Rev. E **94**, 062905 (2016).
[49] Daniel J. Lacks and Mark J. Osborne, Energy Landscape Picture of Overaging and Rejuvenation in a Sheared Glass, Phys. Rev. Lett. **93**, 255501 (2004).
[50] Andrew M. Kraynik, Douglas A. Reinelt, and Frank van Swol, Structure of Random Foam, Phys. Rev. Lett. **93**, 208301 (2004).
[51] Pallabi Das, Anshul D. S. Parmar, and Srikanth Sastry, Annealing glasses by cyclic shear deformation, J. Chem. Phys. **157**, 044501 (2022).
[52] K. A. Newhall, L. L. Pontani, I. Jorjadze, S. Hilgenfeldt, and J. Brujic, Size-Topology Relations in Packings of Grains, Emulsions, Foams, and Biological Cells, Phys. Rev. Lett. **108**, 268001 (2012).
[53] Matthew P. Miklius and Sascha Hilgenfeldt, Analytical Results for Size-Topology Correlations in 2D Disk and Cellular Packings, Phys. Rev. Lett. **108**, 015502 (2012).
[54] Sangwoo Kim, Muyun Cai, and Sascha Hilgenfeldt, Lewis law revisited: The role of anisotropy in size topology correlations, New J. Phys. **16**, 015024 (2014).